METHODS

Comparison of ADS-B Verification Methods: Direct TDOA and MLAT

JUNICHI NAGANAWA , (Member, IEEE), AND HIROMI MIYAZAKI
Electronic Navigation Research Institute (ENRI), National Institute of Maritime, Port and Aviation Technology (MPAT), Tokyo 181-0004, Japan
Corresponding author: Junichi Naganawa (naganawa@mpat.go.jp)

ABSTRACT Automatic Dependent Surveillance—Broadcast (ADS-B) is an emerging means of aeronautical surveillance for air traffic control. Aircraft periodically broadcast positional updates to ground stations. Although ADS-B outperforms traditional radars in terms of accuracy and update rate, positional verification—a technique used to check the validity of the position report—is necessary to counter anomalies. In this study, two different methods were compared when the ground stations measure time difference of arrival (TDOA). One is direct; the test statistic is essentially the difference between the measurement and a prediction calculated from the position report. Another method is multilateration (MLAT)-based and two-step; the emitter position is firstly estimated, whereupon the difference between the estimated and reported positions constitutes the test statistic. As a result of the comparison, a performance difference, which depending on the number of receivers, was revealed. This is an useful suggestion for implementing ADS-B when the existing multilateration infrastructure is exploited.

INDEX TERMS Automatic dependent surveillance—broadcast (ADS-B), multilateration (MLAT), time difference of arrival (TDOA).

I. INTRODUCTION

Automatic Dependent Surveillance-Broadcast (ADS-B) is an emerging means of aeronautical surveillance for air traffic control, which outperforms conventional radars in terms of accuracy, update rate. ADS-B is one of the important components in the global air navigation plan [1]. Aircraft periodically broadcast positional updates to ground stations, which are then collected via a network to the central processor. Deployment of ADS-B has been carried out worldwide [2], [3], [4], [5], [6]. However, ADS-B is dependent on aircraft for position source and also open system without autentication and encryption. Therefore, anomalies due to avionics troubles [7], [8] or illegal transmissions [9], [10], [11], [12] have been concerned.

Various countermeasures have been proposed so far, which have been categorized into positional veification[1] and broadcast authentication [13], [14], [15]. Among them, a promising candidate for air navigation service providers is positional vereification that uses time difference of arrival (TDOA) [16],

The associate editor coordinating the review of this manuscript and approving it for publication was Tariq Umer .

[1] [13], [14], [15] call it secure location verification.

[17], [18], [19], [20], [21]. The receivers measure the TDOA of the ADS-B signal and use it for verifying the positional information inside the signal. Compared with other methods, the TDOA-based method has the following advantages.

1) Compared to broadcast authentication [22], [23], [24], [25], [26], [27], the TDOA-based method eliminates the need for avionics upgrade and standardization process.
2) Intrusion detection using a transponder fingerprint [28], [29], [30], [31] can detect a transmission by an adversary but may overlook a false position due to avionics failure, which is transmitted by an aircraft. The TDOA-based method can detect the both cases as lomg as the reported position deviates from the true position.
3) Unlike other position verification methods [32], [33], [34], [35], implementation onto the existing systems called multilateration (MLAT) [5], [39], [40], [41], [42], [43], [44], [45] is possible without any significant change, and ideally, with only a software upgrade of the central processor. This is of benefit for air navigation service providers.

4) Compared with radar-based verification [18], [36], [37], no radar is needed.
5) To exploit time of arrival (TOA), the timing of signal transmission is needed but not available in ADS-B. On the other hand, TDOA does not require the timing of signal transmission.

We focus on scope to coexist with ADS-B and MLAT (the 3rd item above), because this is what inspired the current work. MLAT is an another means of aeronautical surveillance for air traffic control, which also outperforms conventional radars. Implementation in Frankfurt airspace [5], [40] and Austrian airspace [41] are well known examples. Unlike ADS-B, MLAT does not rely on positional reports but estimates the aircraft position independently based on TDOA measured at multiple ground stations (usually more than three). Both ADS-B and MLAT use the same signal format called Mode-S. Accordingly, ground stations and networks can be shared between ADS-B and MLAT, provided TDOA-based positional verification is employed for ADS-B. The function of the central processor differs. Accordingly, if an MLAT system exists, TDOA-based ADS-B positional verification can be implemented without significant change. However, in such cases, two possible approaches to positional verification can be considered: direct and MLAT-based methods. The former directly uses the difference between measurements and predictions as calculated from the reported position for a test statistic. The latter takes two steps; firstly estimating the emitter position (the aircraft or adversary), then using the difference between estimated and reported positions to calculate the test statistic.

The two methods have not yet been fully investigated in literature particularly from a theoretical perspective. Only brief discussion is available in [16] and [17]. In most studies [21], [23], [37], [38], [39], [40], [41], [42], [43], [44], [45], only either of the two methods was investigated. Otherwise, the main focus is not comparison [19], [20], or detail is not disclosed [18]. Given that merely comparing the two methods is insufficient, it is not known which method should be selected upon system implementation.

Accordingly, in this study, a direct method and an MLAT-based method were compared using statistical theory. Two methods were formulated within the same theoretical framework, where the test statistic, its distribution, and the probability of detection were derived. Both methods were then compared based on the derived formulas. The result depends on the number of receivers N. When $N < 4$, only the direct method is available. When $N = 4$, the two methods perform practically identically. When $N > 4$, the two methods may differ in performance due to different degrees of freedom. A numerical calculation is needed to compare, for which the derived formula can be used. In the scenario presented, the MLAT-based method showed superior performance. The above result suggests that switching the method adaptively depending on N may improve performance.

The rest of the paper is organized as follows: the following subsection provides literature review. Section II introduces

the system model followed by Sections III and IV, direct and MLAT-based methods, respectively. Section V features a comparison based on Sections III and IV. Finally, in Section VI, a numerical simulation is presented to verify the derived formulas and numerically compare the two methods. Section VII concludes the paper.

A. STUDIES RELATED TO TDOA AND MLAT
In [16], as an improvement of a direct method, a solution of the minimum distance between the ADS-B position and the TDOA-hyperbola was derived. In [17], a direct method was proposed, where measurement was processed by a Kalman-filter for time-synchronization then the filter output was used for positional verification. In [16] and [17], a direct method was said to be more advantageous in the number of receivers. However, it was not discussed which method should be selected if the both methods are available. In [18], two methods were evaluated through prototype development by manufacturers, thereby being likely to contribute to current and future implementations. However, detail of [18] is not available. In [19], performance improvement on TDOA-based localization and positional verification was achieved by data-driven techniques and a participatory sensor network. In [20], the data-driven TDOA-method was improved in privacy and efficiency by introducing an encryption scheme. However, comparison between the two methods is not the main focus of [19], [20]. In [21], a theoretical model for a direct method was proposed and verified with measurement, but no MLAT-based method was considered.

In [37], a framework for integrating ADS-B, MLAT, and radars was proposed, where metrics of ADS-B were applied to interpret the performance of MLAT and radars. In [38], the principle of MLAT was applied to air-to-air surveillance. Expected performance was assessed for an uniform distribution of aircraft. In [39] and [23], a MLAT method was proposed and integrated into a holistic security framework. In [40] and [41], implementation and evaluation of wide area MLAT systems for Frankfurt airspace [40] and for Austrian airspace [41] was described. In [42], data fusion and fault detection using MLAT and ADS-B was proposed, where aircraft dynamics and Kalman filter were employed. In [44], [45], and [43], performance improvements of MLAT by exploiting angle-of-arrival [43], [45], frequency-difference-of-arrival [43], and altitude information [44] were proposed. In [23], [37], [38], [39], [41], [42], [43], [44], [45], and [40], a direct method was not considered. In [46], a comparison was made when it was possible to measure distance, but TDOA was not considered.

II. SYSTEM MODEL
A. NOTATION
$x \sim \mathcal{N}(\mu, \Sigma)$ denotes that the variable x follows a Gaussian distribution with mean μ and covariance matrix Σ. $x \sim \chi^2(m)$ denotes that x follows a chi-squared distribution with the degree of freedom m. $x \sim \chi^2(m, \delta)$ denotes that x

follows a noncentral chi-squared distribution with the degree of freedom m and the noncentrality parameter δ. A tilde ~ is used to indicate a measurement value or an estimated value.

B. SYSTEM MODEL

There assumed to be an aircraft and N ground stations. Let $\boldsymbol{r}_i = [x_i, y_i, z_i]^\mathrm{T}$ and $\boldsymbol{l} = [x_1, y_1, z_1]^\mathrm{T}$ be the positions of the ith ground station and the true aircraft position, respectively. The aircraft transmits a position report and let $\boldsymbol{l}' = [x_1', y_1', z_1']^\mathrm{T}$ be the reported position. Each ground station measures the time of arrival (TOA) of the position report. The differences of the TOA between one receiver (called a reference) and the other receivers are the time difference of arrival (TDOA). Here the 1st receiver is assumed be the reference without loosing generosity. Let t_i be the TOA at the ith receiver and $t_{i,1}$ be the TDOA between the ith receiver and the 1th receiver as the reference. Let t_tx be the time when the aircraft starts transmission.

A function that calculates the time of signal propagation between ith ground station and a position, $\boldsymbol{r} = [x, y, z]^\mathrm{T}$, is defined as follows:

$$f_i(\boldsymbol{r}) = \frac{\sqrt{(x - x_i)^2 + (y - y_i)^2 + (z - z_i)^2}}{c}. \quad (1)$$

where c is the speed of propagation. A function $g_{i,1}$, which computes the TDOA, is defined by

$$g_{i,1} = f_i(x, y, z) - f_1(x, y, z). \quad (2)$$

These functions allow the true TOA, t_i, and true TDOA, $t_{i,1}$, to be calculated as follows:

$$t_i = f_i(\boldsymbol{l}) + t_\mathrm{tx} \quad (3)$$
$$t_{i,1} = g_{i,1}(\boldsymbol{l}). \quad (4)$$

In practice, the measurement contains an error. The TOA measurement and the error contained at the ith receiver are denoted by $\tilde{t}_i$ and ϵ_i, respectively:

$$\tilde{t}_i = t_i + \epsilon_i = f_i(\boldsymbol{l}) + t_\mathrm{tx} + \epsilon_i. \quad (5)$$

The TDOA measurement and the contained error are denoted by $\tilde{t}_{i,j}$ and $\epsilon_{i,j}$, respectively:

$$\begin{aligned}
\tilde{t}_{i,1} &= \tilde{t}_i - \tilde{t}_1 \\
&= (t_i + \epsilon_i) - (t_1 + \epsilon_1) \\
&= f_i(\boldsymbol{l}) - f_1(\boldsymbol{l}) + \underbrace{\epsilon_i - \epsilon_1}_{\epsilon_{i,1}} \\
&= g_{i,1}(\boldsymbol{l}) + \epsilon_{i,1}. \quad (6)
\end{aligned}$$

The TOA error is assumed as Gaussian with the standard deviation of the error σ_t:

$$\epsilon_i \sim \mathcal{N}(0, \sigma_t^2). \quad (7)$$

Also assuming that the TOA error is uncorrelated, the TDOA error can be characterized in the form of a vector as follows:

$$\boldsymbol{\epsilon} = \begin{bmatrix} \epsilon_{2,1} & \epsilon_{3,1} & \cdots & \epsilon_{N,1} \end{bmatrix}^\mathrm{T} \sim \mathcal{N}(\boldsymbol{0}, \boldsymbol{V}) \quad (8)$$

$$\boldsymbol{V} = \sigma_t^2 \begin{bmatrix} 2 & 1 & \cdots & 1 \\ 1 & 2 & \cdots & 1 \\ \vdots & \vdots & \ddots & \vdots \\ 1 & 1 & \cdots & 2 \end{bmatrix}. \quad (9)$$

$\boldsymbol{V}$ is positive definite, the proof of which is attached in Appendix B-A. The difference between actual and reported positions is denoted by $\boldsymbol{\Delta}_l$:

$$\boldsymbol{l}' = \boldsymbol{l} + \boldsymbol{\Delta}_l. \quad (10)$$

The assumption regarding $\boldsymbol{\Delta}_l$ depends on whether the position report is valid or not. To model this, two hypotheses are introduced: $\mathcal{H}_0$ (the reported position is valid) and $\mathcal{H}_1$ (the reported position is anomalous). Under $\mathcal{H}_0$, the reported position is around the true position with an error due to self-localization or localization-transmission latency. $\boldsymbol{\Delta}_l$ is assumed as follows:

$$\boldsymbol{\Delta}_l \sim \mathcal{N}(\boldsymbol{0}, \boldsymbol{W}) \quad (11)$$

Because $\boldsymbol{W}$ is a covariance matrix, $\boldsymbol{W}$ is a positive semidefinite. Conversely, under $\mathcal{H}_1$ the reported position is far apart from the true position. $\boldsymbol{\Delta}_l$ is assumed to be a deterministic value, denoted by $\boldsymbol{\Delta}_{l,\mathcal{H}1}$, as follows:

$$\boldsymbol{\Delta}_l = \boldsymbol{\Delta}_{l,\mathcal{H}1}. \quad (12)$$

$\boldsymbol{\Delta}_{l,\mathcal{H}1}$ is subject to the intention of the adversary or the type of navigation system failures, which hampers the statistical characterization. Accordingly, $\boldsymbol{\Delta}_{l,\mathcal{H}1}$ is assumed to be numerically changed.

III. DIRECT METHOD FOR POSITIONAL VERIFICATION

This section derives the direct method.

A. DETECTION LOGIC

The TDOA measured at the ground station are compared with those calculated from the position report. The difference is denoted by $\Delta_{t,i}$ for the pair of the ith and reference receivers and its measurement $\tilde{\Delta}_{t,i}$ is written as follows:

$$\tilde{\Delta}_{t,i} = \tilde{t}_{i,1} - g_{i,1}(\boldsymbol{l}'). \quad (13)$$

Substituting (6) and applying the Taylor series approximation (Appendix A-A), (13) is written as follows:

$$\begin{aligned}
\tilde{\Delta}_{t,i} &= g_{i,1}(\boldsymbol{l}) - g_{i,1}(\boldsymbol{l}') + \epsilon_{i,1} \\
&= -\boldsymbol{a}_{i,1}^\mathrm{T} \boldsymbol{\Delta}_l + \epsilon_{i,1}, \quad (14)
\end{aligned}$$

where $\boldsymbol{a}_{i,1}$ is the coefficient for the approximation. From (8), (9), (11) and (14), $\tilde{\Delta}_{t,i}$ under $\mathcal{H}_0$ is characterized as a Normal distribution as follows:

$$\Delta_{t,i} \sim \mathcal{N}(0, \boldsymbol{a}_{i,1}^\mathrm{T} \boldsymbol{W} \boldsymbol{a}_{i,1} + 2\sigma_t^2). \quad (15)$$

Vectors comprising $\Delta_{t,i}$ and $\tilde{\Delta}_{t,i}$ are introduced as follows:

$$\begin{aligned}
\boldsymbol{\Delta}_t &= \begin{bmatrix} \Delta_{t,2} & \cdots & \Delta_{t,N} \end{bmatrix}^\mathrm{T} \\
\tilde{\boldsymbol{\Delta}}_t &= \begin{bmatrix} \tilde{\Delta}_{t,2} & \cdots & \tilde{\Delta}_{t,N} \end{bmatrix}^\mathrm{T} \quad (16)
\end{aligned}$$

With (16), (14) is written in the form of a vector as follows.

$$\tilde{\boldsymbol{\Delta}}_t = -A\boldsymbol{\Delta}_l + \boldsymbol{\epsilon}$$
$$A = \begin{bmatrix} \boldsymbol{a}_{2,1} & \boldsymbol{a}_{3,1} & \cdots & \boldsymbol{a}_{N,1} \end{bmatrix}^{\mathrm{T}} \quad (17)$$

From (8), (9), (11), and (17), $\tilde{\boldsymbol{\Delta}}_t$ under $\mathcal{H}_0$ is characterized as follows:

$$\tilde{\boldsymbol{\Delta}}_t \sim \mathcal{N}(\boldsymbol{\mu}_{\tilde{\boldsymbol{\Delta}}t,\mathcal{H}0}, \boldsymbol{\Sigma}_{\tilde{\boldsymbol{\Delta}}t,\mathcal{H}0})$$
$$\boldsymbol{\mu}_{\tilde{\boldsymbol{\Delta}}t,\mathcal{H}0} = \mathbf{0}$$
$$\boldsymbol{\Sigma}_{\tilde{\boldsymbol{\Delta}}t,\mathcal{H}0} = AWA^{\mathrm{T}} + V. \quad (18)$$

$\boldsymbol{\Sigma}_{\tilde{\boldsymbol{\Delta}}t,\mathcal{H}0}$ is a positive definite as proven in Appendix B-B. A positive definite matrix is non-singular and invertible according to Theorem 8.1.4 and Lemma 14.2.8 [47], which means a test statistic can be designed as follows:

$$T_{\mathrm{direct}} = \tilde{\boldsymbol{\Delta}}_t^{\mathrm{T}} \boldsymbol{\Sigma}_{\tilde{\boldsymbol{\Delta}}t,\mathcal{H}0}^{-1} \tilde{\boldsymbol{\Delta}}_t. \quad (19)$$

Using [52, Th. A.1], T_{direct} follows a chi-square distribution:

$$T_{\mathrm{direct}} \sim \chi^2(N-1) \quad (20)$$

Therefore, by comparing T_{direct} with the threshold γ_{direct}, the decision can be made as follows:

if $T_{\mathrm{direct}} \leq \gamma_{\mathrm{direct}}$ decides $\mathcal{H}_0$ (Valid Position)
if $T_{\mathrm{direct}} > \gamma_{\mathrm{direct}}$ decides $\mathcal{H}_1$ (Anomaly Position). (21)

γ_{direct} can be decided from (20) such that a constant probability of a false alarm is obtained.

B. MECHANISM OF ANOMALY DETECTION
Substituting (6), (10), (12) into (13) yields

$$\tilde{\Delta}_{t,i} = g_{i,1}(\boldsymbol{l}) - g_{i,1}(\boldsymbol{l}') + \epsilon_{i,1}$$
$$= -\underbrace{\left[g_{i,1}(\boldsymbol{l} + \boldsymbol{\Delta}_{l,\mathcal{H}1}) - g_{i,1}(\boldsymbol{l}) \right]}_{\Delta_{t,i,\mathcal{H}1}} + \epsilon_{i,1} \quad (22)$$

where $\Delta_{t,i,\mathcal{H}1}$ was introduced as a term expressing the effect of the anomaly on the TDOA. With (16), (22) is written in the form of a vector as follows:

$$\tilde{\boldsymbol{\Delta}}_t = -\boldsymbol{\Delta}_{t,\mathcal{H}1} + \boldsymbol{\epsilon}$$
$$\boldsymbol{\Delta}_{t,\mathcal{H}1} = \begin{bmatrix} \Delta_{t,2,\mathcal{H}1} & \cdots & \Delta_{t,N,\mathcal{H}1} \end{bmatrix}^{\mathrm{T}}. \quad (23)$$

With (8), (9), (12) and (23), $\tilde{\boldsymbol{\Delta}}_t$ under $\mathcal{H}_1$ is characterized as follows.

$$\tilde{\boldsymbol{\Delta}}_t \sim \mathcal{N}(\boldsymbol{\mu}_{\tilde{\boldsymbol{\Delta}}t,\mathcal{H}1}, \boldsymbol{\Sigma}_{\tilde{\boldsymbol{\Delta}}t,\mathcal{H}1})$$
$$\boldsymbol{\mu}_{\tilde{\boldsymbol{\Delta}}t,\mathcal{H}1} = -\boldsymbol{\Delta}_{t,\mathcal{H}1}$$
$$\boldsymbol{\Sigma}_{\tilde{\boldsymbol{\Delta}}t,\mathcal{H}1} = V \quad (24)$$

Comparing (24) and (18), one important difference is that $\tilde{\boldsymbol{\Delta}}_t$ is zero-mean under $\mathcal{H}_0$ and not zero-mean under $\mathcal{H}_1$, which means the distribution of the test statistic T_{direct}, as given in (19), is noncentral. Accordingly, the logic in (21) can detect $\mathcal{H}_1$. In more detail, the distribution and non-centrality can be derived as follows.

1) SPECIAL CASE
An special case is $W = 0$, where the derivation is explicit. Substituting $W = 0$ into (18) and (24) yields

$$\boldsymbol{\Sigma}_{\tilde{\boldsymbol{\Delta}}t,\mathcal{H}0} = \boldsymbol{\Sigma}_{\tilde{\boldsymbol{\Delta}}t,\mathcal{H}1} = V. \quad (25)$$

This enables [52, Th. A.1] to be applied with (19) and (24), which yields

$$T_{\mathrm{direct}} \sim \chi^2(N-1, \delta_{\mathrm{direct}})$$
$$\delta_{\mathrm{direct}} = \boldsymbol{\Delta}_{t,\mathcal{H}1}^{\mathrm{T}} V^{-1} \boldsymbol{\Delta}_{t,\mathcal{H}1}. \quad (26)$$

2) GENERAL CASE
When $W \neq 0$, the derivation is not explicit. Instead, the theorem in Appendix A-B enables the distribution of T_{direct} to be calculated as the weighted sum of chi-square distributions. Importantly, the non-centrality is given by substituting $\boldsymbol{\mu}_{\tilde{\boldsymbol{\Delta}}t,\mathcal{H}1}$ into $\boldsymbol{\mu}_x$ in (56).

C. PERFORMANCE METRIC
The detection performance is measured by the probability of anomaly detection, which is denoted as P_{D}. When the probability distribution of T_{direct} is denoted by $p_{\mathrm{direct}}(x)$, P_{D} is calculated by integrating $p_{\mathrm{direct}}(x)$ above the threshold as follows:

$$P_{\mathrm{D}} = \int_{\gamma_{\mathrm{direct}}}^{\infty} p_{\mathrm{direct}}(x) \, \mathrm{d}x. \quad (27)$$

With the result of Section III-B1 and III-B2, P_{D} can be numerically evaluated.

IV. MLAT-BASED METHOD
This section derives the MLAT-based method.

A. LOCALIZATION
A well known MLAT localization scheme is reviewed [48], [49]. The method assumes an initial guess, $\boldsymbol{l}_0$, which is obtained by, for example, a close-form method [50]. By introducing the difference between the true and initial positions $\boldsymbol{\Delta}_{l0} = \boldsymbol{l} - \boldsymbol{l}_0$, a Taylor-series approximation around $\boldsymbol{l}_0$ is obtained as follows:

$$g_{i,1}(\boldsymbol{l}) \approx g_{i,1}(\boldsymbol{l}_0) + \boldsymbol{a}_{i,1}^{\mathrm{T}}(\boldsymbol{l} - \boldsymbol{l}_0). \quad (28)$$

Substituting (6) into (28) yields

$$\boldsymbol{a}_{i,1}^{\mathrm{T}}(\boldsymbol{l} - \boldsymbol{l}_0) + \epsilon_{i,1} = \tilde{t}_{i,1} - g_{i,1}(\boldsymbol{l}_0). \quad (29)$$

With the $N-1$ measurements, the following linear model is obtained:

$$A\boldsymbol{\Delta}_{l0} + \boldsymbol{\epsilon} = \boldsymbol{b} \quad (30)$$
$$\boldsymbol{b} = \begin{bmatrix} \tilde{t}_{2,1} - g_{2,1}(\boldsymbol{l}_0) & \cdots & \tilde{t}_{N,1} - g_{N,1}(\boldsymbol{l}_0) \end{bmatrix}^{\mathrm{T}}. \quad (31)$$

According to [51], a solution is obtained by

$$\tilde{\boldsymbol{\Delta}}_{l0} = \underbrace{(A^{\mathrm{T}} V^{-1} A)^{-1}}_{P} A^{\mathrm{T}} V^{-1} \boldsymbol{b}. \quad (32)$$

Whether $A^{\mathrm{T}} V^{-1} A$ is invertible depends on the rank of A, which is determined by the number of receivers and the

locations. If rank$(A) = 3$, $A^TV^{-1}A$ is invertible, the proof of which is attached in Appendix B-C. This condition, however, can be addressed by appropriately designating receiver positions provided sufficient receivers are available ($N \geq 4$). Therefore, in the rest of this section, it is assumed that rank$(A) = 3$. It is also noted that the inverse, here denoted by P, corresponds to the covariance matrix of the localization error.

B. APPLICATION TO POSITIONAL VERIFICATION

The above localization scheme is applied to positional verification. To do so, the reported position, l', is substituted into the initial position, l_0, whereupon, Δ_{l0} becomes equivalent to $-\Delta_l$. Accordingly, the estimation of the position difference, Δ_l, is given as follows:

$$\begin{aligned} \tilde{\Delta}_l &= -\tilde{\Delta}_{l0} \\ &= -PA^TV^{-1}b. \end{aligned} \tag{33}$$

The statistical characteristic of $\tilde{\Delta}_l$ is examined. Under $\mathcal{H}_0$, substituting (6) and $l_0 = l'$ and applying the Taylor series approximation, the ith element of b in (31) can be written as follows:

$$\begin{aligned} b_i &= \tilde{t}_{i,1} - g_{i,1}(l_0) \\ &= -a_{i,1}^T\Delta_l + \epsilon_{i,1}. \end{aligned} \tag{34}$$

Eq. (34) is written in a vector from as follows:

$$b = -A\Delta_l + \epsilon. \tag{35}$$

With (8), (9), (11) and (35), b under $\mathcal{H}_0$ is characterized as follows:

$$\begin{aligned} b &\sim \mathcal{N}(\mu_{b,\mathcal{H}0}, \Sigma_{b,\mathcal{H}0}) \\ \mu_{b,\mathcal{H}0} &= 0 \\ \Sigma_{b,\mathcal{H}0} &= AWA^T + V. \end{aligned} \tag{36}$$

The derivation of $\Sigma_{b,\mathcal{H}0}$ is attached in Appendixes B-D. With (33) and (36), $\tilde{\Delta}_l$ is characterized as follows:

$$\begin{aligned} \tilde{\Delta}_l &\sim \mathcal{N}(\mu_{\tilde{\Delta}l,\mathcal{H}0}, \Sigma_{\tilde{\Delta}l,\mathcal{H}0}) \\ \mu_{\tilde{\Delta}l,\mathcal{H}0} &= 0 \\ \Sigma_{\tilde{\Delta}l,\mathcal{H}0} &= W + P. \end{aligned} \tag{37}$$

The derivation of $\Sigma_{\tilde{\Delta}l,\mathcal{H}0}$ is attached in Appendix B-E. $\Sigma_{\tilde{\Delta}l,\mathcal{H}0}$ is a positive definite as proven in Appendix B-F, thereby being non-singular and invertible.

Based on these characteristics, a test statistic can be designed as follows:

$$T_{\mathrm{mlat}} = \tilde{\Delta}_l^T \Sigma_{\tilde{\Delta}l,\mathcal{H}0}^{-1} \tilde{\Delta}_l. \tag{38}$$

Using [52, Th. A.1], T_{mlat} under $\mathcal{H}_0$ follows a chi-square distribution:

$$T_{\mathrm{mlat}} \sim \chi^2(3). \tag{39}$$

The degree of freedom is 3 because the position is three dimensional. By comparing T_{mlat} with the threshold γ_{mlat}, the decision can be made as follows:

> if $T_{\mathrm{mlat}} \leq \gamma_{\mathrm{mlat}}$ decides $\mathcal{H}_0$ (Valid Position)
> if $T_{\mathrm{mlat}} > \gamma_{\mathrm{mlat}}$ decides $\mathcal{H}_1$ (Anomaly Position). (40)

γ_{mlat} can be decided from (39) such that a constant probability of a false alarm is obtained.

C. MECHANISM OF ANOMALY DETECTION

Under $\mathcal{H}_1$, substituting (12) into (35) yields

$$b = -A\Delta_{l,\mathcal{H}1} + \epsilon \tag{41}$$

With (8), (9) and (41), b is characterized as follows:

$$b \sim \mathcal{N}(-A\Delta_{l,\mathcal{H}1}, V). \tag{42}$$

With (33) and (42), $\tilde{\Delta}_l$ under $\mathcal{H}_1$ is characterized as follows:

$$\begin{aligned} \tilde{\Delta}_l &\sim \mathcal{N}(\mu_{\tilde{\Delta}l,\mathcal{H}1}, \Sigma_{\tilde{\Delta}l,\mathcal{H}1}) \\ \mu_{\tilde{\Delta}l,\mathcal{H}1} &= \Delta_{l,\mathcal{H}1} \\ \Sigma_{\tilde{\Delta}l,\mathcal{H}1} &= P \end{aligned} \tag{43}$$

The derivation of $\mu_{\tilde{\Delta}l,\mathcal{H}1}$ and $\Sigma_{\tilde{\Delta}l,\mathcal{H}1}$ are attached in Appendixes B-G and B-H, respectively.

Comparing (37) and (43), one important difference is that $\tilde{\Delta}_l$ is zero-mean under $\mathcal{H}_0$ and not zero-mean under $\mathcal{H}_1$, which renders the distribution of T_{mlat}, as given in (38), noncentral. Accordingly, the logic in (40) can detect $\mathcal{H}_1$. In more detail, the distribution of T_{mlat} and non-centrality can be derived as follows:

1) SPECIAL CASE

An special case is when $W = 0$, where the derivation is explicit. Substituting $W = 0$ into (37) and (43) yields

$$\Sigma_{\tilde{\Delta}l,\mathcal{H}0} = \Sigma_{\tilde{\Delta}l,\mathcal{H}1} = P. \tag{44}$$

This enables [52,Th. A.1] to be applied with (38) and (43), which yields

$$\begin{aligned} T_{\mathrm{mlat}} &\sim \chi^2(3, \delta_{\mathrm{mlat}}) \\ \delta_{\mathrm{mlat}} &= \Delta_{l,\mathcal{H}1}^T P^{-1} \Delta_{l,\mathcal{H}1}. \end{aligned} \tag{45}$$

2) GENERAL CASE

When $W \neq 0$, the derivation is not explicit. Instead, the theorem in Appendix A-B enables the distribution of T_{mlat} to be calculated as the weighted sum of chi-square distributions. The non-centrality is given by substituting $\mu_{\tilde{\Delta}l,\mathcal{H}1}$ into μ_x in (56).

D. ANOMALY DETECTION PERFORMANCE

Like the direct method, i.e. (27), P_D is calculated by integrating the probability distribution of T_{mlat} above γ_{mlat}.

V. COMPARISON

Based on the derivations in Sections III and IV, the two methods were compared. The comparison focused on availability and performance, which, in turn, depends on the number of receivers.

A. N < 4

In this case, the MLAT-based method is unavailable and only the direct method is available. Although this disadvantage of MLAT has been known [17], the contribution of this paper is that it proves the advantage of the direct method against the MLAT-based method.

To show this, the matrix inverses, which regulate the availability, were examined. The direct method involves $\mathbf{\Sigma}_{\tilde{\Delta}t, \mathcal{H}0}^{-1}$, but $\mathbf{\Sigma}_{\tilde{\Delta}t, \mathcal{H}0}$ is a positive definite and always invertible as proven in Appendix B-B. Thus, the direct method is always available, including the $N < 4$ case. Conversely, the MLAT-based method is unavailable because $A^{\mathrm{T}}V^{-1}A$, which is a 3×3 matrix, becomes rank-deficient. This can be proven by combining the following equations:

$$\mathrm{rank}(A^{\mathrm{T}}V^{-1}A) \leq \mathrm{rank}(A) \tag{46}$$

$$\mathrm{rank}(A) \leq \min(N - 1, 3) \tag{47}$$

$$N < 4 \tag{48}$$

where (46) was derived by [47, Corollary 4.4.5].

B. N = 4

In this case, the direct method is available, as is the MLAT-based method provided $\mathrm{rank}(A) = 3$. Although the availability of the MLAT-based method remains constrained, it is expected that the condition will be satisfied by designing the receiver locations appropriately. Accordingly, the focus of comparison is detection performance. In a nutshell, the two methods show practically identical performance, which can be shown as follows:

First, the two methods have identical distribution of the test statistic under $\mathcal{H}_0$. This can be shown by substituting $N = 4$ into (20) and comparing it with (39). Next, $\mathcal{H}_1$ is examined. For comparison, the following Taylor series approximation is considered.

$$\mathbf{\Delta}_{t, \mathcal{H}1} = A\mathbf{\Delta}_{l, \mathcal{H}1} \tag{49}$$

Substituting (49) into (26) and (45) yields

$$\begin{aligned}\delta_{\mathrm{direct}} &= \mathbf{\Delta}_{t, \mathcal{H}1}^{\mathrm{T}} V^{-1} \mathbf{\Delta}_{t, \mathcal{H}1}. \\ &= (A\mathbf{\Delta}_{l, \mathcal{H}1})^{\mathrm{T}} V^{-1} A\mathbf{\Delta}_{l, \mathcal{H}1}. \\ &= \mathbf{\Delta}_{l, \mathcal{H}1}^{\mathrm{T}} A^{\mathrm{T}} V^{-1} A\mathbf{\Delta}_{l, \mathcal{H}1}. \end{aligned} \tag{50}$$

$$\begin{aligned}\delta_{\mathrm{mlat}} &= \mathbf{\Delta}_{l, \mathcal{H}1}^{\mathrm{T}} P^{-1} \mathbf{\Delta}_{l, \mathcal{H}1} \\ &= \mathbf{\Delta}_{l, \mathcal{H}1}^{\mathrm{T}} (A^{\mathrm{T}} V^{-1} A) \mathbf{\Delta}_{l, \mathcal{H}1} \end{aligned} \tag{51}$$

(50) and (51) indicate that non-centrality becomes the same. Substituting $N = 4$ into (26) and (45) also yields the same degree of freedom. Thus, T_{direct} and T_{mlat} have identical distribution and the probability of detection becomes the same.
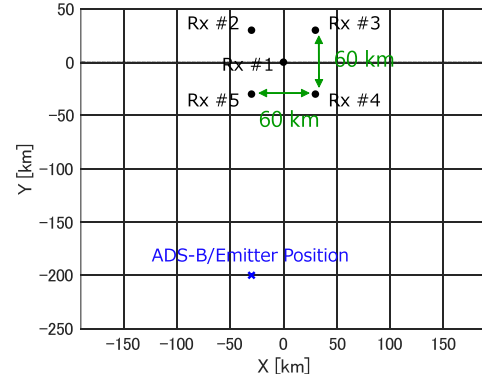

FIGURE 1. Simulation setup of Scenario A.

It is noted that the above discussion assumes the Taylor series approximation, which can be inaccurate for a large value of $\mathbf{\Delta}_{l, \mathcal{H}1}$. However, in that case the probability of detection will approach 1, rendering the difference between the two methods negligible. Accordingly, the two methods show practically identical performance. Also noted for the discussion above is the assumption that $W = 0$. The case for $W \neq 0$ is evaluated numerically in Section VI, where the two methods show identical performance.

C. N > 4

Here, the two methods perform differently, due to differing degrees of freedom. Comparing the probability of detection requires numerical calculation and the derivation is as follows:

Under $\mathcal{H}_0$, the two methods follow a chi-square distribution with different degrees of freedom; $N - 1$ for the direct method and 3 for the MLAT-based method, respectively, as shown in (20) and (39). Under $\mathcal{H}_1$, the two methods follow a noncentral chi-square distribution. The non-centrality is the same, as shown in (50) and (51), but the degree of freedom differs, as shown in (26) and (45). Also noted is the fact that the above discussion assumes $W = 0$. The case for $W \neq 0$ is evaluated numerically in Section VI.

VI. NUMERICAL SIMULATION

Simulations were conducted to verify the derived formulas and numerically compare both methods. Three simulation scenarios were considered: A, B, and C.

A. SCENARIO A

Scenario A mainly focused on verifying the derived formulas and five receivers and an emitter were considered. Fig. 1 shows the receiver (labeled as "Rx") positions and the position for the emitter or ADS-B. This arrangement was designed as receivers located in a continent and an oceanic airspace. Receiver #1 was located at the origin and the other receivers were located at the corner of the rectangle, with edges of 60 km and its center at the origin. The receivers were on the ground. The ADS-B/emitter position was at $[-30 \text{ km}, -200 \text{ km}, 9144 \text{ m} (30,000 \text{ feet})]$, which was not
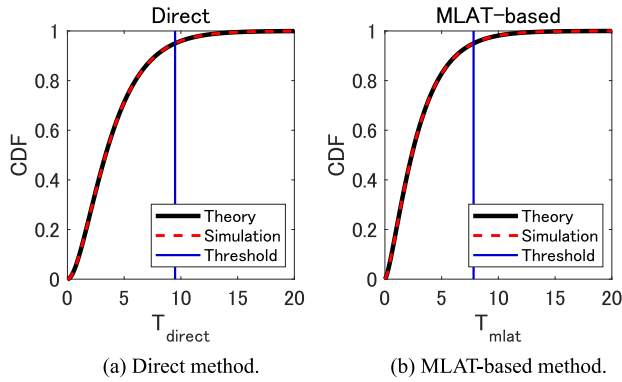
FIGURE 2. Simulation result for $\mathcal{H}_0$ of Scenario A: $W \neq 0$.

FIGURE 3. Simulation result for $\mathcal{H}_1$ of Scenario A: $W = 0$.

surrounded by the receivers and elicited conservative configuration in terms of expected performance.

Two types of simulations were conducted: namely $\mathcal{H}_0$ and $\mathcal{H}_1$. In the $\mathcal{H}_0$ simulation, the emitter position was fixed. For each trial, measurements and an ADS-B position were generated according to (6)–(11). Based on the trials, the test statistics, probability of a false alarm and threshold were all evaluated. In the $\mathcal{H}_1$ simulation, the ADS-B position was also fixed. The emitter was also fixed but deviated from the reported position by giving $\Delta_{l,\mathcal{H}1}$. In each trial, measurements were generated according to (6)–(10) and (12) detection logics was also applied. Based on the trials, the test statistics and probability of detection were evaluated.

$\sigma_t = 13.9$ ns was selected based on [21]. Two cases of W were considered: $W = 0$ and $W \neq 0$. For $W \neq 0$, W is assumed as follows:

$$W = \text{diag}(\sigma_x^2, \sigma_y^2, \sigma_z^2) \tag{52}$$

The lack of correlation among x, y and z is assumed, given the difficulty in deciding on the correlation parameters in reality. $\sigma_x = 75.6$ m and $\sigma_y = 75.6$ m were selected based on the accuracy requirement of [55], where Navigation Accuracy Category for Position (NACp) of 7 is required for a separation of five nautical miles.[2] $\sigma_z = 173.1$ m were selected based on σ_x, σ_y and the yearly statistics of the horizontal/vertical dilution of precision reported in [56]. $\Delta_{l,\mathcal{H}1} = [1852\text{ m}, 0, 0]$ (1 nautical mile) was selected based on [55], which also requires the detection of significant ADS-B error by a secondary surveillance radar.

B. RESULT

1) CONFORMATION UNDER $\mathcal{H}_0$

Fig. 2 shows the distribution of the test statistic, where the $W \neq 0$ case was selected as a representative example. Lines labeled as ''Theory'' correspond to $\chi^2(N-1)$ for the direct method, as derived in (20) and $\chi^2(3)$ for the MLAT-based method, as derived in (39), respectively. Effective agreement with the simulation result (the lines labeled as ''Simulation'')

---

²It is noted that σ_x and σ_y differed from the authors' previous work [21], where measurement data were used to decide the parameters.
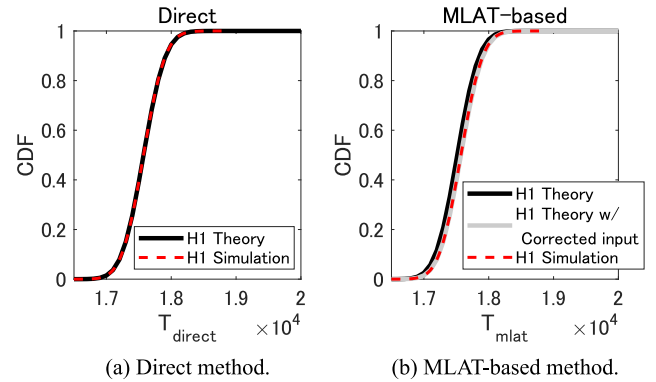
was observed, which meant the derived formulas were confirmed.

From the test statistic distribution, the thresholds were obtained such that the probability of a false alarm was 0.05. For the direct method, both simulation and theory obtained $\gamma_{\text{direct}} = 9.5$, showing positive correlation. For the localization-based method, both simulation and theory obtained $\gamma_{\text{mlat}} = 7.8$, also showing agreement. Conformation was made for $W = 0$ but omitted for brevity.

2) CONFORMATION UNDER $\mathcal{H}_1$

Fig. 3 shows the test statistic distribution for $W = 0$ under $\mathcal{H}_1$. Lines labeled as ''H1 Theory'' corresponds to $\chi^2(N, \delta_{\text{direct}})$ for the direct method, as derived in (26) and $\chi^2(3, \delta_{\text{mlat}})$ for the localization-based method, as derived in (45), respectively, Compared with $\mathcal{H}_0$ (Fig. 2), the test statistics under $\mathcal{H}_1$ are significantly larger, allowing the anomaly to be detected. The probability of detection was 1.0 for both simulation and theory, regardless of the method used.

Good agreement with the simulation (labeled as ''H1 Simulation'') was also observed for the direct method, thereby confirming the derived formulas. However, slight disagreement was observed for the MLAT-based method; the median of T_{mlat} differed by 0.4 % between the simulation and theory. The reason and correction were investigated, which is available in Appendix C. The reason identified was that the MLAT method did not obtain an unbiased solution due to the Taylor series approximation. As a result of the correction, the new theoretical line labeled as ''H1 Theory w/ Corrected Input'' was obtained, which correlates well with the simulation. In practical terms, however, the impact of this disagreement is negligible because the test statistic was sufficiently high and the probability of detection was 1.0

The case for $W \neq 0$ was also confirmed in the same manner. Fig. 4 shows the result. The main difference is that the lines labeled as ''H1 Theory'' were calculated following Sections III-B2, Section IV-C2, and Appendix A-B. Effective agreement with the simulation was also observed for the direct method. Slight disagreement was observed for the MLAT-based method for the same reason as in the $W = 0$
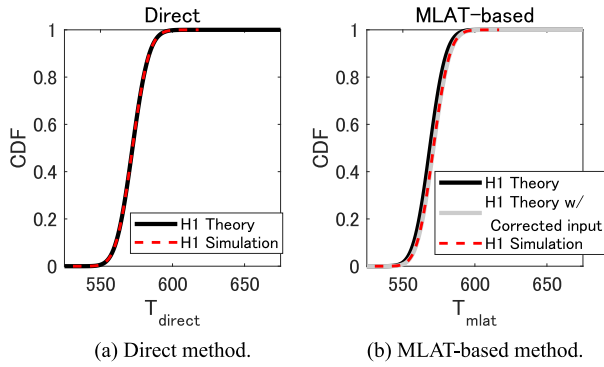
(a) Direct method. (b) MLAT-based method.

FIGURE 4. Simulation result for $\mathcal{H}_1$ of Scenario A: $W \neq 0$.

FIGURE 5. Simulation setup of Scenario B.

FIGURE 6. Probability of detection for $N = 3$ of Scenario B.
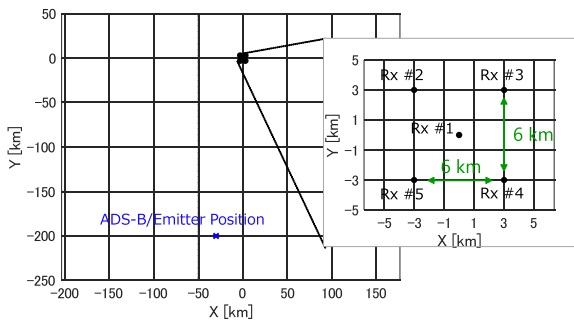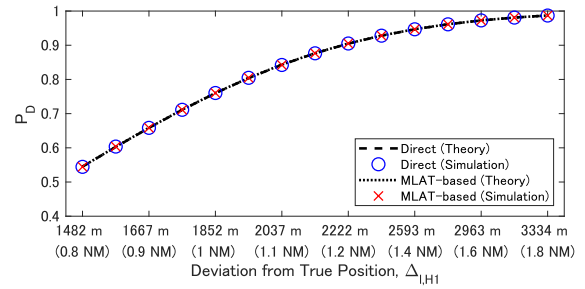

FIGURE 7. Probability of detection for $N = 4$ of Scenario B.

case. The probability of detection was 1.0 for both simulation and theory regardless of the method.

C. SCENARIO B

Scenario B mainly focuses on comparing two methods. The simulation setup in Scenario B was set to be harsher than that in Scenario A because Scenario A showed effective probability of detection for both methods without any difference. In particular, the distances between the receivers were shortened, as shown in Fig. 5. Changing the receiver distances was inspired from the prior knowledge on Dilution of Precision (DOP), which has been widely used to examine localization accuracy [41], [43], [44], [57], [58]. DOP represents geometrical effect on accuracy. DOP is good in area surrounded by receivers but poor in outer area. Therefore, in order to deteriorate the performance, a shorter distance was introduced, which results in a larger outer area. In a practical sense, the arrangement can be interpreted such that receivers located in an island monitor an oceanic airspace. The TDOA accuracy was also degraded to $\sigma_t = 50.0$ ns, which can be interpreted as the use of a low-cost receiver. $N = 5$ (an example of $N > 4$), $N = 4$ and $N = 3$ (an example of $N < 4$) are evaluated; Rx #5 is removed for $N = 4$ and Rx #4 and #5 are removed for $N = 3$.

D. RESULT
1) COMPARISON FOR $N = 3$ (An EXAMPLE OF $N < 4$)
As discussed in Section V-A, the MLAT-based method is inapplicable due to rank-deficiency. Actually, the numerical
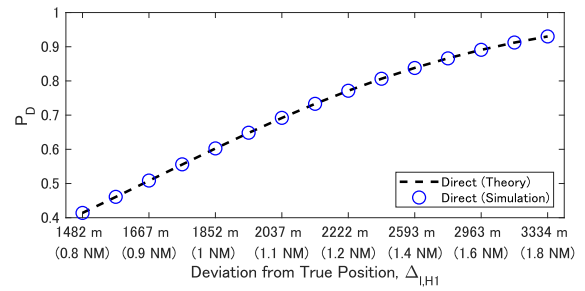
computation of the test statistic was unsuccessful, although the direct method was applicable. The probability of detection is shown in Fig. 6. Accordingly, when $N < 4$, the direct method is the only choice. Agreement between the theory and simulation was also confirmed.

2) COMPARISON FOR $N = 4$
As discussed in Section V-B, the two methods are expected to show practically identical performance. This was confirmed in Fig. 7, where both methods showed agreement in term of the probability of detection. Further, the parameters of the test statistic distribution were compared. Because the distribution is a weighted sum of (noncentral) chi-squared distributions, the non-centrality and weight of each component is compared as shown in Figs. 8(a) and (b). The parameters also agreed between the two methods, so identical performance from both methods was confirmed.

It is added that agreement between the theory and simulation was also confirmed in Fig. 7.

3) COMPARISON FOR $N = 5$ (An EXAMPLE OF $N > 4$)
As discussed in Section V-C, the two methods are expected to differ in performance. Fig. 9 compares the probability of detection, where the MLAT-based method showed a better performance. To investigate why, the parameters of the test statistic distribution were compared as shown in Fig. 10(a) and (b), whereupon agreement in the weight coefficients and non-centrality parameters was observed. The difference was in the number of components, which can be interpreted equivalently as the difference in the degree of freedom because all the weight coefficients are almost 1. The improved preformance of the MLAT-based method can be intuitively understood as a result of the difference on how to
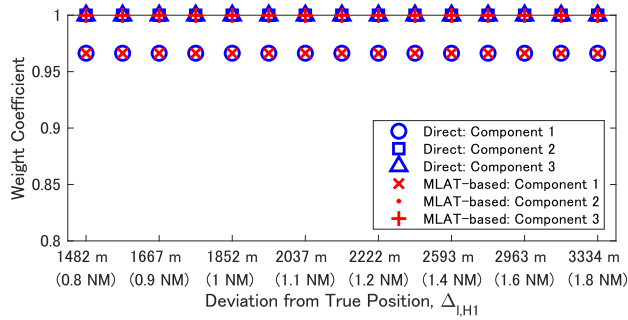
(a) Weight coefficient.
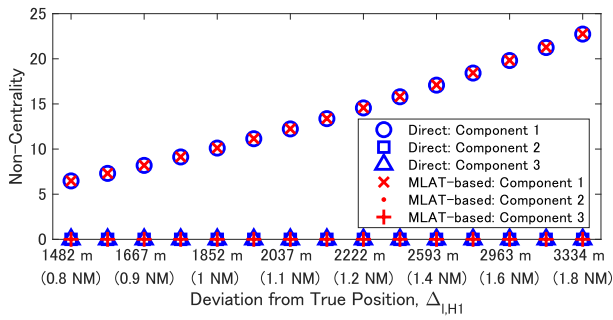
(b) Non-centrality.

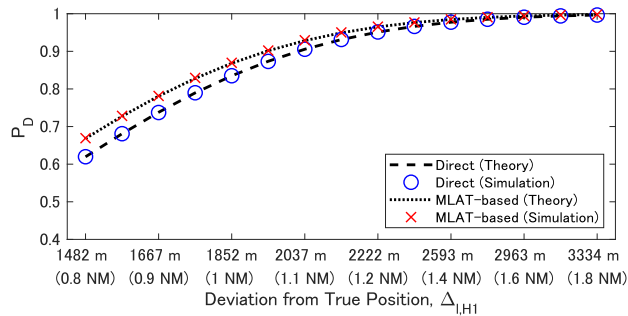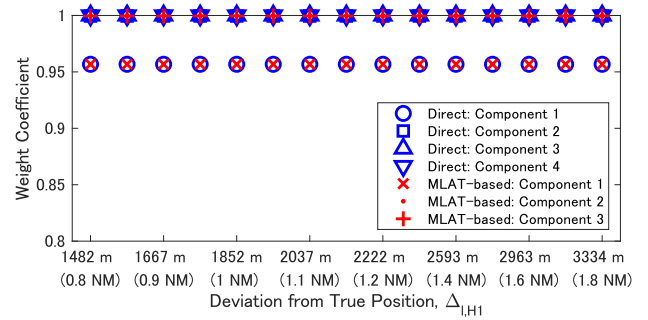**FIGURE 8.** Parameters of test statistic distribution for *N* = 4 of Scenario B.

FIGURE 9. Probability of detection for *N* = 5 of Scenario B.

exploit prior knowledge on the problem. There is a cause-and-effect relationship between a positional difference (cause) and TDOA-differences (effect). The direct-based method only examines the effect, whereas the MLAT-based method tries to estimate the cause. As a result, the MLAT-based method obtains an improvement if successful.
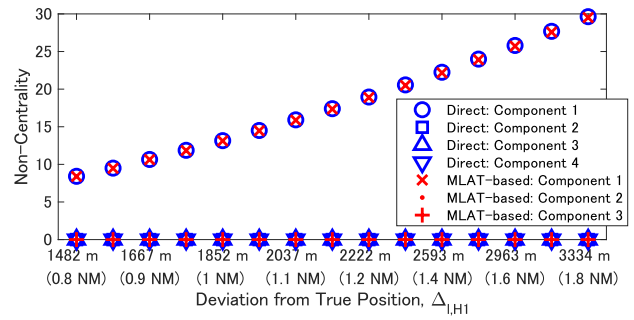
E. SCENARIO C

Scenario C demonstrates that the derived formula can be easily extended for a moving case. The parameters were the same as Scenario B with $N = 5$ except that the ADS-B and the emitter positions under $\mathcal{H}_1$. A moving trjectory was simulated as the collection of $M(= 7)$ ADS-B positions as shown Fig. 11.

The derived formulat and numerical simulation was applied to each position. This produced the probability of detection at the mth position, which is denoted by $P_D(m)$ and plotted in Fig. 12. The average over the trajectory

(a) Weight coefficient.

(b) Non-centrality.

FIGURE 10. Parameters of test statistic distribution for *N* = 5 of Scenario B.
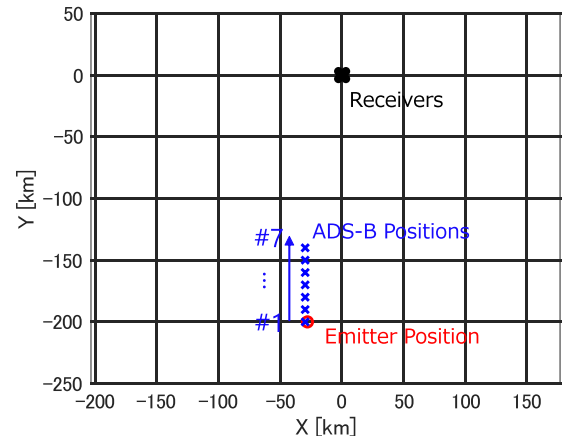
FIGURE 11. Simulation setup of Scenario C.

TABLE 1. Average probability of detection.

Method	Theory	Simulation
Direct	0.93	0.93
MLAT-based	0.94	0.94

was then calculated by

$$\bar{P}_D = \frac{1}{M}\sum_{m=1}^{M} P_D(m) \tag{53}$$

Table 1 summarizes the result. Agreement between the theory and simulation was observed. Also, the MLAT-based method showed a better performance. Thus, the derived formula can be applied to a moving case.

FIGURE 12. Probability of detection for Scenario C.

VII. CONCLUSION

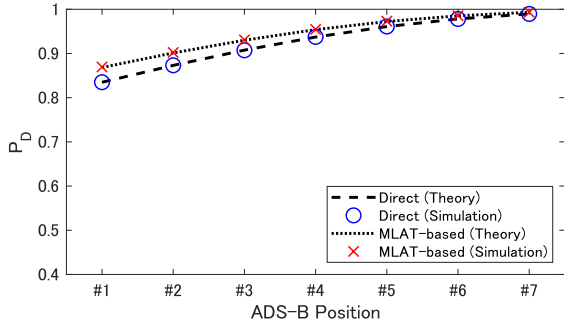The direct method and MLAT-based method of ADS-B positional verification were compared. Using statistical theory, the test statistic and its distribution were derived, so that the detection threshold and probability of detection could be determined. The difference of the two methods depends on the number of receivers, N. When $N < 4$, only the direct method is available. When $N = 4$, the two methods have practically identical performance. When $N > 4$, the performance of the two methods may differ due to the degree of freedom. An actual comparison requires numerical calculation, for which the derived formula can be used. In the presented scenario, the MLAT-based method showed superior performance. The result above suggests switching the method adaptively depending on N for a better performance.

APPENDIX A
THEOREMS

This section introduces some mathematical results that are frequently used.

A. TAYLOR SERIES APPROXIMATION OF TDOA

A Taylor series approximation of $g_{i,1}(l)$ around l' is given as follows:

$$
\begin{aligned}
g_{i,1}(l) &\approx g_{i,1}(l') + a_{i,1}^{\mathrm{T}}(l - l') \\
&\approx g_{i,1}(l') - a_{i,1}^{\mathrm{T}} \Delta_l
\end{aligned}
$$

$$
a_{i,1} = \left[\left.\frac{\partial g_{i,1}}{\partial x}\right|_{r=l'} \quad \left.\frac{\partial g_{i,1}}{\partial y}\right|_{r=l'} \quad \left.\frac{\partial g_{i,1}}{\partial z}\right|_{r=l'} \right]^{\mathrm{T}}. \quad (54)
$$

B. QUADRATIC FORM IN NORMAL VARIABLES (General Case)

For $x \sim \mathcal{N}(\mu_x, \Sigma_x)$, the quadratic form $T = x^{\mathrm{T}} C x$ is considered where $C \neq \Sigma_x^{-1}$ and C is a positive semidefinite and symmetric. To obtain the Cumulative Distribution Function (CDF) of T, computing is necessary [53], [54]. To do so, the quadratic form can be rewritten as follows [53]:

$$
T = z^{\mathrm{T}} \Lambda z \quad (55)
$$

where $z \sim \mathcal{N}(\mu_z, I)$ and Λ is a diagonal matrix. This result says T is the same as a weighted sum of independent,

potentially noncentral, chi-squared random variables. The computing procedure is as follows:

1) By the Cholesky decomposition of Σ, $\Sigma^{1/2}$ such that $\Sigma = \Sigma^{1/2}(\Sigma^{1/2})^{\mathrm{T}}$ is calculated.
2) $M = (\Sigma^{1/2})^{\mathrm{T}} C \Sigma^{1/2}$ is calculated.
3) The eigenvalues of M, the diagonal matrix of the eigenvalues Λ and the orthonormal matrix such that $M = Q \Lambda Q_{\mathrm{T}}$ are calculated.
4) μ_z is given by

$$
\mu_z = Q^{\mathrm{T}} (\Sigma^{1/2})^{-1} \mu_x. \quad (56)
$$

5) The CDF in the form of (55) can be calculated according to [54].

APPENDIX B
DERIVATIONS
A. DEFINITENESS OF V

V can be written as follows:

$$
V = \sigma_t^2 (I + J) \quad (57)
$$

where I is the identity matrix and J is the matrix, the elements of which are all one. I is positive definite and J is a positive semidefinite, so V is positive definite [47].

B. DEFINITENESS OF $\Sigma_{\tilde{\Delta}t, \mathcal{H}0}$

The two terms constituting $\Sigma_{\tilde{\Delta}t, \mathcal{H}0}$ are examined. The first term $A W A^{\mathrm{T}}$ is a non-negative definite because W is positive semidefinite and Theorem 14.2.9 [47] can be applied. The second term V is a positive definite, making. $\Sigma_{\tilde{\Delta}t, \mathcal{H}0}$ is a positive definite, according to Lemma 14.2.4 [47].

C. INVERSION OF $A^{\mathrm{T}} V^{-1} A$

First, V^{-1} is considered. V^{-1} is a positive definite because V is a positive definite as proven in Appendix B-A and [47, Corollary 14.2.11] is applicable. Additionally, rank(A) = 3 is considered. Then, using [47, Th. 14.2.9], [47, Lemma 14.2.8], and [47, Th. 8.1.4], $A^{\mathrm{T}} V^{-1} A$ is a positive definite and invertible. The inverse, $P = (A^{\mathrm{T}} V^{-1} A)^{-1}$ also becomes a positive definite.

D. DERIVATION OF $\Sigma_{\tilde{\Delta}l, \mathcal{H}0}$

$\Sigma_{b, \mathcal{H}0}$ was derived as follows:

$$
\begin{aligned}
\Sigma_{b, \mathcal{H}0} &= \mathrm{E}\left[(b - \mu_{b, \mathcal{H}0})(b - \mu_{b, \mathcal{H}0})^{\mathrm{T}}\right] \\
&= \mathrm{E}\left[b b^{\mathrm{T}}\right] \\
&= \mathrm{E}\left[(A \Delta_l + \epsilon)(A \Delta_l + \epsilon)^{\mathrm{T}}\right] \\
&= A \mathrm{E}\left[\Delta_l \Delta_l^{\mathrm{T}}\right] A^{\mathrm{T}} + \mathrm{E}\left[\epsilon \epsilon^{\mathrm{T}}\right] \\
&= A W A^{\mathrm{T}} + V.
\end{aligned} \quad (58)
$$

E. DERIVATION OF $\Sigma_{\tilde{\Delta}l, \mathcal{H}0}$

$\Sigma_{\tilde{\Delta}l, \mathcal{H}0}$ was derived as follows.

$$
\Sigma_{\tilde{\Delta}l, \mathcal{H}0} = \mathrm{E}\left[(\tilde{\Delta}_l - \mu_{\tilde{\Delta}l, \mathcal{H}0})(\tilde{\Delta}_l - \mu_{\tilde{\Delta}l, \mathcal{H}0})^{\mathrm{T}}\right]
$$

$$= \mathrm{E}\left[\tilde{\boldsymbol{\Delta}}_l \tilde{\boldsymbol{\Delta}}_l^{\mathrm{T}}\right]$$

$$= \mathrm{E}\left[\boldsymbol{P}\boldsymbol{A}^{\mathrm{T}}\boldsymbol{V}^{-1}\boldsymbol{b}\left\{\boldsymbol{P}\boldsymbol{A}^{\mathrm{T}}\boldsymbol{V}^{-1}\boldsymbol{b}\right\}^{\mathrm{T}}\right]$$

$$= \mathrm{E}\left[\boldsymbol{P}\boldsymbol{A}^{\mathrm{T}}\boldsymbol{V}^{-1}\boldsymbol{b}\boldsymbol{b}^{\mathrm{T}}(\boldsymbol{V}^{-1})^{\mathrm{T}}\boldsymbol{A}\boldsymbol{P}^{\mathrm{T}}\right]$$

$$= \boldsymbol{P}\boldsymbol{A}^{\mathrm{T}}\boldsymbol{V}^{-1}\boldsymbol{\Sigma}_{b,\mathcal{H}0}(\boldsymbol{V}^{-1})^{\mathrm{T}}\boldsymbol{A}\boldsymbol{P}^{\mathrm{T}}$$

$$= \boldsymbol{P}\boldsymbol{A}^{\mathrm{T}}\boldsymbol{V}^{-1}(\boldsymbol{A}\boldsymbol{W}\boldsymbol{A}^{\mathrm{T}} + \boldsymbol{V})(\boldsymbol{V}^{-1})^{\mathrm{T}}\boldsymbol{A}\boldsymbol{P}^{\mathrm{T}}$$

$$= \boldsymbol{P}(\boldsymbol{A}^{\mathrm{T}}\boldsymbol{V}^{-1}\boldsymbol{A})\boldsymbol{W}\boldsymbol{A}^{\mathrm{T}}(\boldsymbol{V}^{-1})^{\mathrm{T}}\boldsymbol{A}\boldsymbol{P}^{\mathrm{T}}$$
$$\quad + \boldsymbol{P}\boldsymbol{A}^{\mathrm{T}}(\boldsymbol{V}^{-1})^{\mathrm{T}}\boldsymbol{A}\boldsymbol{P}^{\mathrm{T}}$$

$$= \boldsymbol{W}(\boldsymbol{A}^{\mathrm{T}}\boldsymbol{V}^{-1}\boldsymbol{A})^{\mathrm{T}}\boldsymbol{P}^{\mathrm{T}} + \boldsymbol{P}(\boldsymbol{A}^{\mathrm{T}}\boldsymbol{V}^{-1}\boldsymbol{A})^{\mathrm{T}}\boldsymbol{P}^{\mathrm{T}}$$

$$= \boldsymbol{W} + \boldsymbol{P}. \tag{59}$$

F. DEFINITENESS OF $\Sigma_{\tilde{\Delta}l,\mathcal{H}0}$

The two terms constituting $\boldsymbol{\Sigma}_{\tilde{\Delta}l,\mathcal{H}0}$ are examined. The first term $\boldsymbol{W}$ is positive semidefinite. The second term $\boldsymbol{P}$ is positive definite as long as rank$(\boldsymbol{A}) = 3$. Then, $\boldsymbol{\Sigma}_{\tilde{\Delta}l,\mathcal{H}0}$ is positive definite, according to Lemma 14.2.4 [47].

G. DERIVATION OF $\mu_{\tilde{\Delta}l,\mathcal{H}1}$

$\boldsymbol{\mu}_{\tilde{\Delta}l,\mathcal{H}1}$ was derived as follows:

$$\boldsymbol{\mu}_{\tilde{\Delta}l,\mathcal{H}1} = \mathrm{E}[\tilde{\boldsymbol{\Delta}}_l]$$
$$= -\boldsymbol{P}\boldsymbol{A}^{\mathrm{T}}\boldsymbol{V}^{-1}\mathrm{E}[\boldsymbol{b}]$$
$$= \boldsymbol{P}\boldsymbol{A}^{\mathrm{T}}\boldsymbol{V}^{-1}\boldsymbol{A}\boldsymbol{\Delta}_{l,\mathcal{H}1}$$
$$= \boldsymbol{\Delta}_{l,\mathcal{H}1} \tag{60}$$

H. DERIVATION OF $\Sigma_{\tilde{\Delta}l,\mathcal{H}1}$

To derive $\boldsymbol{\Sigma}_{\tilde{\Delta}l,\mathcal{H}1}$, the following equation was firstly obtained:

$$\tilde{\boldsymbol{\Delta}}_l - \boldsymbol{\mu}_{\tilde{\Delta}l,\mathcal{H}1} = -\boldsymbol{P}\boldsymbol{A}^{\mathrm{T}}\boldsymbol{V}^{-1}\boldsymbol{b} - \boldsymbol{\Delta}_{l,\mathcal{H}1}$$
$$= -\boldsymbol{P}\boldsymbol{A}^{\mathrm{T}}\boldsymbol{V}^{-1}\left(-\boldsymbol{A}\boldsymbol{\Delta}_{l,\mathcal{H}1} + \boldsymbol{\epsilon}\right) - \boldsymbol{\Delta}_{l,\mathcal{H}1}$$
$$= -\boldsymbol{P}\boldsymbol{A}^{\mathrm{T}}\boldsymbol{V}^{-1}\boldsymbol{\epsilon} \tag{61}$$

Using the equation above, $\boldsymbol{\Sigma}_{\tilde{\Delta}l,\mathcal{H}1}$ was derived as follows:

$$\boldsymbol{\Sigma}_{\tilde{\Delta}l,\mathcal{H}1} = \mathrm{E}\left[(\tilde{\boldsymbol{\Delta}}_l - \boldsymbol{\mu}_{\tilde{\Delta}l,\mathcal{H}1})(\tilde{\boldsymbol{\Delta}}_l - \boldsymbol{\mu}_{\tilde{\Delta}l,\mathcal{H}1})^{\mathrm{T}}\right]$$
$$= \mathrm{E}\left[\boldsymbol{P}\boldsymbol{A}^{\mathrm{T}}\boldsymbol{V}^{-1}\boldsymbol{\epsilon}\boldsymbol{\epsilon}^{\mathrm{T}}\left(\boldsymbol{P}\boldsymbol{A}^{\mathrm{T}}\boldsymbol{V}^{-1}\right)^{\mathrm{T}}\right]$$
$$= \boldsymbol{P}\boldsymbol{A}^{\mathrm{T}}\boldsymbol{V}^{-1}\mathrm{E}\left[\boldsymbol{\epsilon}\boldsymbol{\epsilon}^{\mathrm{T}}\right]\left(\boldsymbol{P}\boldsymbol{A}^{\mathrm{T}}\boldsymbol{V}^{-1}\right)^{\mathrm{T}}$$
$$= \boldsymbol{P}\boldsymbol{A}^{\mathrm{T}}\left(\boldsymbol{P}\boldsymbol{A}^{\mathrm{T}}\boldsymbol{V}^{-1}\right)^{\mathrm{T}}$$
$$= \boldsymbol{P}\boldsymbol{A}^{\mathrm{T}}(\boldsymbol{V}^{-1})^{\mathrm{T}}\boldsymbol{A}\boldsymbol{P}^{\mathrm{T}}$$
$$= \boldsymbol{P}\left(\boldsymbol{A}^{\mathrm{T}}\boldsymbol{V}^{-1}\boldsymbol{A}\right)^{\mathrm{T}}\boldsymbol{P}^{\mathrm{T}}$$
$$= \boldsymbol{P} \tag{62}$$

APPENDIX C
ERROR UNDER $\mathcal{H}_1$ FOR MLAT-BASED METHOD
Slight disagreement between the simulation and theory was observed in Fig. 3 for the MLAT-based method. The reason and correction are explained in this section.
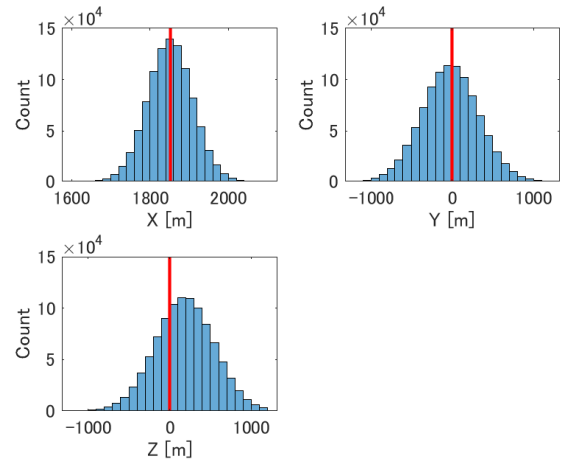

FIGURE 13. Distribution of $\tilde{\boldsymbol{\Delta}}_l$.

A. REASON
The reason identified was the Taylor series approximation, which was used to derive (35) and (41), applicable to a general case and $\mathcal{H}_1$, respectively. The assumption is that the ADS-B position is sufficiently close to the emitter, which may cause an error under $\mathcal{H}_1$. For the case of Fig. 3, the error was evaluated by the following equation:

$$\boldsymbol{\epsilon}_{\text{approx}} = \boldsymbol{b} + \boldsymbol{A}\boldsymbol{\Delta}_{l,\mathcal{H}_1} - \boldsymbol{\epsilon} \tag{63}$$

which was obtained by taking the difference between the left-hand site and the right-hand side in (41). All the terms were available in the simulation. The result was $\boldsymbol{\epsilon}_{\text{approx}} = $ [5.9 ns, 0.6 ns, −2.8 ns, −5.1 ns].

B. CORRECTION
The approximation error further caused a bias in the estimation $\tilde{\boldsymbol{\Delta}}_l$. Fig. 13 shows $\tilde{\boldsymbol{\Delta}}_l$ where x, y, and z components were separately plotted. The red lines indicate the true values, i.e. $\boldsymbol{\Delta}_{l,\mathcal{H}1} = $ [1852 m, 0, 0]. As shown in Fig. 13, a bias was obvious for z-component. The other components are also slightly biased, although they are not so visible. The amount of the bias was then evaluated as follows:

$$\mathrm{E}\left[\tilde{\boldsymbol{\Delta}}_l\right] - \boldsymbol{\Delta}_{l,\mathcal{H}1} = [−0.7 \text{ m}, −21.0 \text{ m}, 184.5 \text{ m}] \tag{64}$$

The bias is related to the non-centrality parameter via (45). Therefore, a correction is possible by substituting the biased estimate, $\mathrm{E}\left[\tilde{\boldsymbol{\Delta}}_l\right]$, instead of the true value, $\boldsymbol{\Delta}_{l,\mathcal{H}1}$. The result is given as the line labeled as "H1 Theory w/ Corrected Input" in Fig. 3, which agreed with the simulation.

It is noted that the above case is for $\boldsymbol{W} = \boldsymbol{0}$, but the same mechanism was also observed for $\boldsymbol{W} \neq \boldsymbol{0}$, i.e. Fig. 4 In this case, a correction was made by substituting the biased estimate into (56).

REFERENCES
[1] *The Global Air Navigation Plan Portal*. Accessed: Jun. 7, 2022. [Online]. Available: https://www4.icao.int/ganpportal/
[2] G. Wright, "NAV Canada implements ADS-B," in *Proc. Integr. Commun., Navigat. Surveill. Conf.*, May 2009, pp. 1–9, doi: 10.1109/ICNSURV.2009.5172868.

[3] E. Boci, S. Sarkani, and T. A. Mazzuchi, "Optimizing ADS-B coverage," in *Proc. Integr. Commun., Navigat. Surveill. Conf.*, May 2009, pp. 1–10, doi: 10.1109/ICNSURV.2009.5172863.

[4] K. Wangchuk, Sangay, J. Naganawa, D. Adhikari, and K. Gayley, "ADS-B Coverage Design in Mountainous Terrain," in *Air Traffic Management and Systems IV* (Lecture Notes in Electrical Engineering), vol. 731. Singapore: Springer, 2019, pp. 327–336, doi: 10.1007/978-981-33-4669-7_19.

[5] S. Stanzel, "DFS ADS-B implementation in high density radar controlled airspace—Experiences and challenges," in *Proc. 7th OpenSky Workshop* (EPiC Series in Computing), vol. 67, C. Popper and M. Strohmeier Eds. Stockport, U.K.: EasyChair, 2019, pp. 1–12, doi: 10.29007/8jkt.

[6] E. Boci, "An end-to-end data driven approach for delivering ATC grade ADS-B services at Truckee Tahoe," in *Proc. Integr. Commun. Navigat. Surveill. Conf. (ICNS)*, Apr. 2021, pp. 1–9, doi: 10.1109/ICNS52807.2021.9441624.

[7] A. Hoag, M. A. Garcia, and J. Dolan, "Identifying collision avoidance resolution advisories and anomalies in aircraft avionics globally with space-based ADS-B data observations," in *Proc. Int. Symp. Enhanced Solutions Aircr. Vehicle Surveill. Appl. (ESAVS)*, Berlin, Germany, Oct. 2018, pp. 1–7.

[8] B. S. Ali, W. Ochieng, A. Majumdar, W. Schuster, and T. K. Chiew, "ADS-B system failure modes and models," *J. Navigat.*, vol. 67, no. 6, pp. 995–1017, Nov. 2014.

[9] L. Purton, H. Abbass, and S. Alam, "Identification of ADS-B system vulnerabilities and threats," in *Proc. Australas. Transp. Res. Forum*, Sep./Oct. 2010, pp. 1–16.

[10] D. McCallie, J. Butts, and R. Mills, "Security analysis of the ADS-B implementation in the next generation air transportation system," *Int. J. Crit. Infrastruct. Protection*, vol. 4, no. 2, pp. 78–87, Jul. 2011.

[11] A. Costin and A. Francillon, "Ghost in the air (traffic): On insecurity of ADS-B protocol and practical attacks on ADS-B devices," in *Proc. Black Hat USA*, Las Vegas, NV, USA, Jul. 2012, pp. 1–12.

[12] S. Khandker, H. Turtiainen, A. Costin, and T. Hamalainen, "On the (in)security of 1090 ES and UAT 978 mobile cockpit information systems—An attacker perspective on the availability of ADS-B safety- and mission-critical systems," *IEEE Access*, vol. 10, pp. 37718–37730, 2022, doi: 10.1109/ACCESS.2022.3164704.

[13] M. Strohmeier, V. Lenders, and I. Martinovic, "On the security of the automatic dependent surveillance-broadcast protocol," *IEEE Commun. Surveys Tuts.*, vol. 17, no. 2, pp. 1066–1086, 2nd Quart., 2015.

[14] M. R. Manesh and N. Kaabouch, "Analysis of vulnerabilities, attacks, countermeasures and overall risk of the automatic dependent surveillance-broadcast (ADS-B) system," *Int. J. Crit. Infrastruct. Protection*, vol. 19, pp. 16–31, Dec. 2017.

[15] Z. Wu, T. Shang, and A. Guo, "Security issues in automatic dependent Surveillance–Broadcast (ADS-B): A survey," *IEEE Access*, vol. 8, pp. 122147–122167, 2020.

[16] G. Graziano, P. De Marco, F. Perilli, and L. Mene, "TDOA based ADS-B validation," in *Proc. ESAVS*, Berlin, Germany, Mar. 2013.

[17] M. Leonardi, "ADS-B anomalies and intrusions detection by sensor clocks tracking," *IEEE Trans. Aerosp. Electron. Syst.*, vol. 55, no. 5, pp. 2370–2381, Oct. 2019, doi: 10.1109/TAES.2018.2886616.

[18] *Final Project Report Surveillance Ground System Enhancements for ADS-B (Prototype Development)*, SESAR Joint Undertaking, Brussels, Belgium, May 2015.

[19] M. Strohmeier, V. Lenders, and I. Martinovic, "Lightweight location verification in air traffic surveillance networks," in *Proc. Workshop Cyber-Phys. Syst. Secur.*, Apr. 2015, pp. 49–60.

[20] H. Yang, Q. Zhou, D. Liu, H. Li, and X. Shen, "AEALV: Accurate and efficient aircraft location verification for ADS-B," *IEEE Trans. Cognit. Commun. Netw.*, vol. 7, no. 4, pp. 1399–1411, Dec. 2021, doi: 10.1109/TCCN.2021.3072853.

[21] J. Naganawa and H. Miyazaki, "Theory of automatic dependent surveillance–broadcast position verification using time difference of arrival," *IEEE Trans. Aerosp. Electron. Syst.*, vol. 57, no. 3, pp. 1387–1404, Jun. 2021, doi: 10.1109/TAES.2020.3043536.

[22] C. Finke, J. Butts, R. Mills, and M. Grimaila, "Enhancing the security of aircraft surveillance in the next generation air traffic control system," *Int. J. Crit. Infrastruct. Protection*, vol. 6, no. 1, pp. 3–11, Mar. 2013.

[23] T. Kacem, D. Wijesekera, and P. Costa, "ADS-Bsec: A holistic framework to secure ADS-B," *IEEE Trans. Intell. Vehicles*, vol. 3, no. 4, pp. 511–521, Dec. 2018, doi: 10.1109/TIV.2018.2873911.

[24] S. Sciancalepore and R. Di Pietro, "SOS: Standard-compliant and packet loss tolerant security framework for ADS-B communications," *IEEE Trans. Dependable Secure Comput.*, vol. 18, no. 4, pp. 1681–1698, Aug. 2021, doi: 10.1109/TDSC.2019.2934446.

[25] A. Braeken, "Holistic air protection scheme of ADS-B communication," *IEEE Access*, vol. 7, pp. 65251–65262, 2019.

[26] G. Thumbur, N. B. Gayathri, P. V. Reddy, M. Z. U. Rahman, and A. Lay-Ekuakille, "Efficient pairing-free identity-based ADS-B authentication scheme with batch verification," *IEEE Trans. Aerosp. Electron. Syst.*, vol. 55, no. 5, pp. 2473–2486, Oct. 2019.

[27] Z. Wu, A. Guo, M. Yue, and L. Liu, "An ADS-B message authentication method based on certificateless short signature," *IEEE Trans. Aerosp. Electron. Syst.*, vol. 56, no. 3, pp. 1742–1753, Jun. 2020, doi: 10.1109/TAES.2019.2933957.

[28] M. Strohmeier, V. Lenders, and I. Martinovic, "Intrusion detection for airborne communication using PHY-layer information," in *Proc. Int. Conf. Detection Intrusions Malware, Vulnerability Assessment*. Cham, Switzerland: Springer, Jun. 2015, pp. 67–77.

[29] M. Strohmeier and I. Martinovic, "On passive data link layer fingerprinting of aircraft transponders," in *Proc. 1st ACM Workshop Cyber-Phys. Syst.-Secur. PrivaCy*, Denver, CO, USA, Oct. 2015, pp. 1–9.

[30] M. Leonardi, L. Di Gregorio, and D. Di Fausto, "Air traffic security: Aircraft classification using ADS-B message's phase-pattern," *Aerospace*, vol. 4, no. 4, p. 51, Oct. 2017.

[31] M. Leonardi and F. Gerardi, "Aircraft mode s transponder fingerprinting for intrusion detection," *Aerospace*, vol. 7, no. 3, p. 30, Mar. 2020, doi: 10.3390/aerospace7030030.

[32] C. Reck, M. S. Reuther, A. Jasch, and L.-P. Schmidt, "Verification of ADS-B positioning by direction of arrival estimation," *Int. J. Microw. Wireless Technol.*, vol. 4, no. 2, pp. 181–186, Apr. 2012.

[33] W. Wang, G. Chen, R. Wu, D. Lu, and L. Wang, "A low-complexity spoofing detection and suppression approach for ADS-B," in *Proc. Integr. Commun., Navigat. Surveill. Conf. (ICNS)*, Herdon, VA, USA, Apr. 2015, pp. 1–8.

[34] N. Ghose and L. Lazos, "Verifying ADS-B navigation information through Doppler shift measurements," in *Proc. IEEE/AIAA 34th Digit. Avionics Syst. Conf. (DASC)*, Prague, Czech Republic, Sep. 2015, pp. 1–11.

[35] Y. Kim, J.-Y. Jo, and S. Lee, "A secure location verification method for ADS-B," in *Proc. IEEE/AIAA 35th Digit. Avionics Syst. Conf. (DASC)*, Sep. 2016, pp. 1–10, doi: 10.1109/DASC.2016.7778003.

[36] P. Mariano, P. De Marco, and C. Giacomini, "Data integrity augmentation by ADS-B SSR hybrid techniques," in *Proc. Integr. Commun., Navigat., Surveill. Conf. (ICNS)*, Herndon, VA, USA, Apr. 2018, pp. 1–10.

[37] A. Smith, R. Cassell, T. Breen, R. Hulstrom, and C. Evers, "Methods to provide system-wide ADS-B back-up, validation and security," in *Proc. IEEE/AIAA 25th Digit. Avionics Syst. Conf.*, Portland, OR, USA, Oct. 2006, pp. 1–7, doi: 10.1109/DASC.2006.313681.

[38] K. Sampigethaya, "Visualization & assessment of ADS-B security for green ATM," in *Proc. 29th Digit. Avionics Syst. Conf.*, Oct. 2010, pp. 1–16.

[39] M. Monteiro, A. Barreto, R. Division, T. Kacem, J. Carvalho, D. Wijesekera, and P. Costa, "Detecting malicious ADS-B broadcasts using wide area multilateration," in *Proc. IEEE/AIAA 34th Digit. Avionics Syst. Conf. (DASC)*, Sep. 2015, pp. 1–12, doi: 10.1109/DASC.2015.7311413.

[40] H. Neufeldt and S. Stanzel, "An operational WAM in Frankfurt airspace," in *Proc. 14th Int. Radar Symp. (IRS)*, Dresden, Germany, Jun. 2013, pp. 561–566.

[41] W. Langhans, C. Scheiflinger, W. Weidner, J. Auer, P. Fitzgerald, and M. Anzalone, "Implementation of a nationwide wide-area multilateration system for Austrian airspace," in *Proc. Integr. Commun., Navigat. Surveill. Conf. (ICNS)*, Apr. 2013, pp. 1–18, doi: 10.1109/ICNSurv.2013.6548675.

[42] W. Liu, J. Wei, M. Liang, Y. Cao, and I. Hwang, "Multi-sensor fusion and fault detection using hybrid estimation for air traffic surveillance," *IEEE Trans. Aerosp. Electron. Syst.*, vol. 49, no. 4, pp. 2323–2339, Oct. 2013, doi: 10.1109/TAES.2013.6621819.

[43] Y. A. Nijsure, G. Kaddoum, G. Gagnon, F. Gagnon, C. Yuen, and R. Mahapatra, "Adaptive air-to-ground secure communication system based on ADS-B and wide-area multilateration," *IEEE Trans. Veh. Technol.*, vol. 65, no. 5, pp. 3150–3165, May 2016, doi: 10.1109/TVT.2015.2438171.

[44] S.-L. Jheng, S.-S. Jan, Y.-H. Chen, and S. Lo, "1090 MHz ADS-B-based wide area multilateration system for alternative positioning navigation and timing," *IEEE Sensors J.*, vol. 20, no. 16, pp. 9490–9501, Aug. 2020, doi: 10.1109/JSEN.2020.2988514.

[45] D. Zhao, J. Sun, and G. Gui, "En-route multilateration system based on ADS-B and TDOA/AOA for flight surveillance systems," in *Proc. IEEE 91st Veh. Technol. Conf. (VTC-Spring)*, May 2020, pp. 1–6, doi: 10.1109/VTC2020-Spring48590.2020.9129436.

[46] J. Naganawa, "Comparison of direct and localization-based methods for position verification using distance measurement," in *Proc. IEEE Region 10 Conf. (TENCON)*, Dec. 2021, pp. 179–184, doi: 10.1109/TENCON54134.2021.9707224.

[47] D. A. Harville, *Matrix Algebra From A Statistician's Perspective*. Cham, Switzerland: Springer, 2008.

[48] W. H. Foy, "Position-location solutions by Taylor-series estimation," *IEEE Trans. Aerosp. Electron. Syst.*, vol. AES-12, no. 2, pp. 187–194, Mar. 1976.

[49] D. Torrieri, "Statistical theory of passive location systems," *IEEE Trans. Aerosp. Electron. Syst.*, vol. AES-20, no. 2, pp. 183–198, Mar. 1984.

[50] Y. T. Chan and K. C. Ho, "A simple and efficient estimator for hyperbolic location," *IEEE Trans. Signal Process.*, vol. 42, no. 8, pp. 1905–1915, Aug. 1994, doi: 10.1109/78.301830.

[51] S. M. Kay, *Fundamentals of Statistical Signal Processing: Estimation Theory*. Upper Saddle River, NJ, USA: Prentice-Hall, 1993.

[52] M. S. Paolella, *Linear Models and Time-Series Analysis: Regression, ANOVA, ARMA and GARCH*. Hoboken, NJ, USA: Wiley, Nov. 2018, p. 678.

[53] H. Zhang, J. Shen, and Z. Wu, "A fast and accurate approximation to the distributions of quadratic forms of Gaussian variables," *J. Comput. Graph. Statist.*, vol. 31, no. 1, pp. 304–311, Jan. 2022, doi: 10.1080/10618600.2021.2000423.

[54] J. P. Imhof, "Computing the distribution of quadratic forms in normal variables," *Biometrika*, vol. 48, nos. 3–4, pp. 419–426, Dec. 1961.

[55] *Safety, Performance and Interoperability Requirements Document for ADS-B-RAD Application*, EUROCAE, Lucerne, Switzerland, Sep. 2009.

[56] B. A. Renfro, M. Stein, E. B. Reed, J. Morales, and E. J. Villalba, "An analysis of global positioning system (GPS) standard positioning service performance for 2019," Appl. Res. Lab., Univ. Texas, Austin, TX, USA, Tech. Rep. TR-SGL-20-02, May 2020.

[57] A. Jasch, T. Feuerle, G. Scoor, and P. Hecker, "Geometrical siting considerations for wide area multilateration systems," in *Proc. IEEE/ION Position, Location Navigat. Symp.*, May 2010, pp. 1304–1308, doi: 10.1109/PLANS.2010.5507349.

[58] L. Alia, A. Italiano, and F. Pozzi, "Advanced tools to analyze the expected performance of multilateration and wide area multilateration," in *Proc. Tyrrhenian Int. Workshop Digit. Commun. Enhanced Surveill. Aircr. Vehicles (TIWDC/ESAV)*, Sep. 2014, pp. 82–86, doi: 10.1109/TIWDC-ESAV.2014.6945453.

JUNICHI NAGANAWA (Member, IEEE) graduated from the Gifu National College of Technology, Gifu, Japan, in 2007. He received the B.Eng. degree from the Tokyo Institute of Technology, Tokyo, Japan, in 2009, the M.Eng. degree from the University of Tokyo, Tokyo, in 2011, and the D.Eng. degree from the Tokyo Institute of Technology, Tokyo, in 2015. Since 2015, he has been with the Surveillance and Communications Department, Electronic Navigation Research Institute (ENRI), National Institute of Maritime, Port and Aviation Technology (MPAT), Tokyo, where he is currently a Senior Researcher. His research interests include aeronautical communication/surveillance and air-ground radio propagation. He is a member of IEICE. He was a recipient of the Young Researcher's Award of IEICE.

HIROMI MIYAZAKI received the B.Eng. degree in electronic engineering and the M.Eng. degree in electrical and electronic engineering from Shinshu University, Nagano, Japan, in 1991 and 1993, respectively, and the D.Eng. degree from the Nagasaki University, Nagasaki, in 2020. Since 1993, he has been with the Electronic Navigation Research Institute (ENRI), National Institute of Maritime, Port and Aviation Technology, Tokyo, Japan. His research interest includes aeronautical surveillance technologies.

● ● ●